





Enhanced Detection of Single Viruses On-Chip via Hydrodynamic Focusing

Jennifer A. Black , *Student Member, IEEE*, Erik Hamilton , *Student Member, IEEE*, Raúl A. Reyes Hueros, Joshua W. Parks, Aaron R. Hawkins , *Fellow, IEEE*, and Holger Schmidt , *Fellow, IEEE*

Abstract—Planar optofluidics provide a powerful tool for facilitating chip-scale light-matter interactions. Silicon-based liquid core waveguides have been shown to offer single molecule sensitivity for efficient detection of bioparticles. Recently, a PDMS based planar optofluidic platform was introduced that opens the way to rapid development and prototyping of unique structures, taking advantage of the positive attributes of silicon dioxide-based optofluidics and PDMS based microfluidics. Here, hydrodynamic focusing is integrated into a PDMS based optofluidic chip to enhance the detection of single H1N1 viruses on-chip. Chip-plane focusing is provided by a system of microfluidic channels to force the particles towards a region of high optical collection efficiency. Focusing is demonstrated and enhanced detection is quantified using fluorescent polystyrene beads where the coefficient of variation is found to decrease by a factor of 4 with the addition of hydrodynamic focusing. The mean signal amplitude of fluorescently tagged single H1N1 viruses is found to increase with the addition of focusing by a factor of 1.64.

Index Terms—Biophotonics, hydrodynamic focusing, optofluidics, soft photolithography, waveguides.

I. INTRODUCTION

OPTOFLUIDICS is a synergistic field comprised of optics and microfluidics. Planar optofluidic devices enable light-matter interactions on a chip with fluids (e.g., liquids) [1]. Often, such platforms utilize silicon dioxide-based structures which integrate solid-core optical waveguides and fluid filled leaky optical waveguides. These devices have demonstrated sensitive detection of fluorescent particles within a liquid medium down to single bioparticles such as viruses and nucleic acids [2], [3], [4]. However, it has been found that the light collection efficiency off-chip of such devices strongly depends on

the particle's position within the fluidic channel [5]. Particles which reside near the center of the channel are detected more efficiently as their emission better overlaps with the propagating mode within the microfluidic channel. Therefore, it is advantageous to focus the particles near the center of the microfluidic channel for optimal collection efficiency.

Microfluidic devices have been fabricated using a multitude of materials including elastomers [6], thermosets [7], thermoplastics [8], paper [9] and hybrids consisting of combinations of materials [10]. The elastomer polydimethylsiloxane (PDMS) has widely been used for rapid fabrication of microfluidic channels [11] for a host of biological applications [12]. Fluid manipulation is important for chip-based applications and PDMS devices have been used to demonstrate mixing [13], sorting [14], droplet creation [15] and hydrodynamic focusing (HDF) [16]. HDF is appealing for flow cytometry where it is necessary to optically probe single particles in time [17], [18]. Microfluidic channels often operate with low Reynolds number making the flow laminar. This results in a parabolic velocity distribution of the fluid within the channel. Particles flowing through a perpendicular excitation laser in a light induced fluorescence experiment thereby spend more or less time in the excitation beam depending on their speed. Further, the optical mode intensity profile varies within the channel. This results in a distribution of fluorescence intensities. Forcing the particles into a smaller cross-sectional area within the fluidic channel results in a narrower velocity and excitation intensity distribution; thereby resulting in less variation in the emitted fluorescence signal intensities. The quality of the detected signal is quantified by the coefficient of variation (CV) and is calculated by dividing the standard deviation of the signal intensities by the mean of the distribution. The smaller the CV, the more discernible different particle species will be. Recent demonstrations of on-chip multiplexing using multi-mode interference waveguides could benefit from a decrease in CV in order to more efficiently distinguish the resulting fluorescence signals [19], [20].

Integration of PDMS with oxide-based platforms has been demonstrated combining methods for chip-based fluid manipulation/preparation and oxide-based optofluidics [2], [21]. Recently, fully integrated optofluidic devices have been demonstrated with PDMS [22] and other polymers [23]. The aforementioned PDMS devices integrate solid-core total internal reflection based optical waveguides with microfluidic channels which work twofold as leaky optical waveguides. Such PDMS optofluidic devices have been shown to have sufficient sensitivity

Manuscript received April 2, 2018; revised June 10, 2018 and June 20, 2018; accepted June 21, 2018. Date of publication July 9, 2018; date of current version July 23, 2018. This work was funded by NIH under Grants 4R33AI100229 and 1R01AI116989 and the NSF under Grant CBET-1703058. (*Corresponding author: Jennifer A. Black.*)

J. A. Black, R. A. R. Hueros, J. W. Parks, and H. Schmidt are with the School of Engineering, University of California Santa Cruz, Santa Cruz, CA 95064 USA (e-mail: jblack@soe.ucsc.edu; raanrey@ucsc.edu; parksj10@gmail.com; hschmidt@soe.ucsc.edu).

E. Hamilton and A. R. Hawkins are with the Department of Electrical and Computer Engineering, Brigham Young University, Provo, UT 84602 USA (e-mail: erikshamilton08@gmail.com; hawkins@ee.byu.edu).

This paper has supplementary downloadable material available at <http://ieeexplore.ieee.org>. This includes video clips and a PDF of information relevant to this work. This material is 35.5 MB in size.

Color versions of one or more of the figures in this paper are available online at <http://ieeexplore.ieee.org>.

Digital Object Identifier 10.1109/JSTQE.2018.2854574

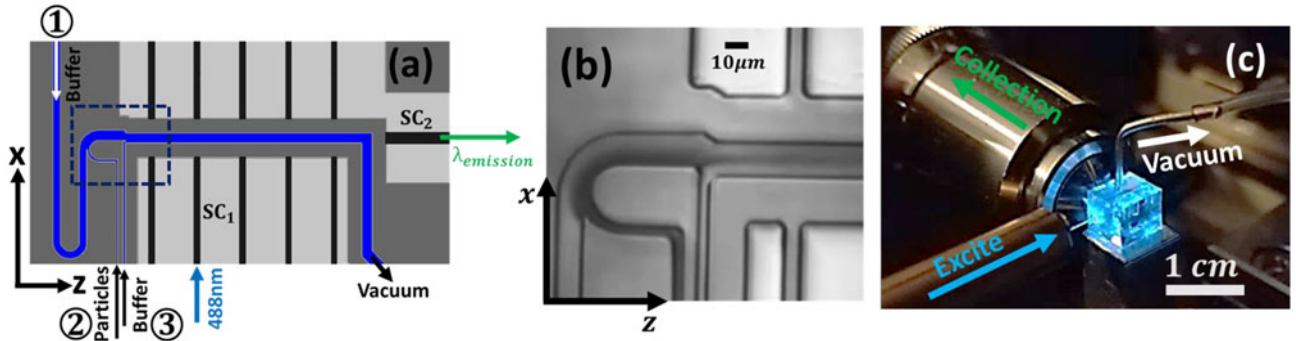


Fig. 1. (a) Schematic of the optofluidic device. Microfluidic channels (solid-core optical waveguides) are shown in blue (black). Three input reservoirs are denoted: 1, 2 and 3. For focusing, reservoir 2 is filled with a particle solution and reservoirs 1 and 3 are filled with a buffer. Vacuum is applied to the shared outlet reservoir to pull the liquids through the channel. A single mode optical fiber launches excitation laser light (488 nm) into a waveguide on chip (SC_1) which guides the light to the microfluidic channel. As particles pass through the excitation beam, they fluoresce, and that light is collected along the z-direction by a multi-mode waveguide for off-chip detection (SC_2). (b) A microscope image of a fabricated device near the triple inlet intersection (region denoted by a dashed box in Fig. 1(a)). Focusing is evident when reservoir 2 is filled with food dye and reservoirs 1 and 3 are filled with DI water. (c) Image of a chip with vacuum line attached, excitation laser aligned and collection objective aligned perpendicular to excitation.

such that single fluorescently stained *E. Coli* bacteria were detected in-plane [22]. Soft photolithography allows for rapid prototyping and the PDMS based planar optofluidic devices require a single photomask ensuring optimal waveguide alignment. Herein, we present a PDMS based optofluidic chip that enables detection of single viruses on-chip. It fully integrates a system of microfluidic channels which provide HDF for a stream of fluorescent particles via negative pressure driven flow. This system of channels is interfaced with solid-core optical waveguides which facilitate enhanced light induced fluorescence detection. Focusing is validated and quantitatively analyzed using fluorescent polystyrene beads. Lastly, HDF enhanced detection of single H1N1 viruses is demonstrated on-chip.

II. METHODS

The system of microfluidic channels designed to provide HDF is fully integrated in-plane with a system of solid-core optical waveguides as seen in Fig. 1(a) where the fluidic channels are shown in blue and the solid-core optical waveguides are shown in black. Fluid which flows from reservoirs 1 and 2 (Fig. 1(a)) intersect just before a ninety degree bend which is designed to provide out of plane (y-direction) focusing of particles due to the creation of a Dean vortex at very high flow speeds [24]. In-plane (x-direction) focusing is provided by a channel offset and sheath flow created by fluid flowing from reservoir 3. A single outlet from the system of microfluidic channels is attached to a vacuum which provides flow from the three inlets via negative pressure (experimentally, -35 inHg). For the designed channel lengths and experimentally accessible negative pressures, the resulting flow speeds are not high enough to provide for Dean focusing. However, in-plane focusing is visually evident in Fig. 1(b) where a microscope image was taken at the microfluidic intersection (dashed box in Fig. 1(a)) after reservoir 2 was filled with food dye and the buffer channels were filled with deionized (DI) water.

The devices were fabricated using soft photolithography [22]. The index of refraction of PDMS depends on the base to curing

agent ratio [25]. The solid-core waveguides and microfluidic channel sidewalls are made of 5:1 (base:curing agent) PDMS and have higher index of refraction than the cladding layers which are made of 10:1 PDMS. The 5:1 was first spun onto a silanized SU-8 master at 6000 RPM for 30 minutes. After curing, 10:1 was poured directly atop the 5:1 layer. Concurrently, a second 10:1 layer was poured onto a silanized blank silicon wafer. After all PDMS was cured, reservoir holes were punched for fluidic access and the wafer was completed by plasma bonding the two pieces together. Individual devices were diced from the wafer using a razor blade. More information on fabrication can be found in the downloadable supplemental material found on <http://ieeexplore.ieee.org>.

To probe for fluorescence, an excitation laser (488 nm) was first coupled into single mode optical fiber (Newport FS-V). The light was then launched into the excitation solid-core waveguide (SC_1 , cross-sectional dimensions $\sim 6 \mu\text{m} \times 5.5 \mu\text{m}$) which guides the light to the microfluidic channel. The particles flow through the excitation volume and fluoresce as they pass through. Their emitted fluorescence signal was collected downstream by a multi-mode solid-core waveguide (SC_2 , cross-sectional dimensions $\sim 6 \mu\text{m} \times 12 \mu\text{m}$) which lies perpendicular to the excitation waveguide. The output was collected from the chip via an objective where it was then filtered and sent to an avalanche photodetector (APD). An image of the chip is found in Fig. 1(c) where the outlet line runs to a vacuum and the excitation fiber and collection objective are aligned. Both commercially available polystyrene beads (FluoSphere) and Alexa Fluor 488 tagged H1N1 viruses were optically excited and detected in-plane. In the polystyrene bead experiments, a video imaging the excitation region from the top was also recorded with an appropriate filter for the excitation laser beam. From the video, the bead positions were determined while from the APD trace, the signal heights and speeds of the particles were extracted. Simulations of particle trajectories were carried out using finite element analysis, optical mode profiles were simulated using PhotonDesign's FIMMWAVE and all data analysis was performed in Matlab.

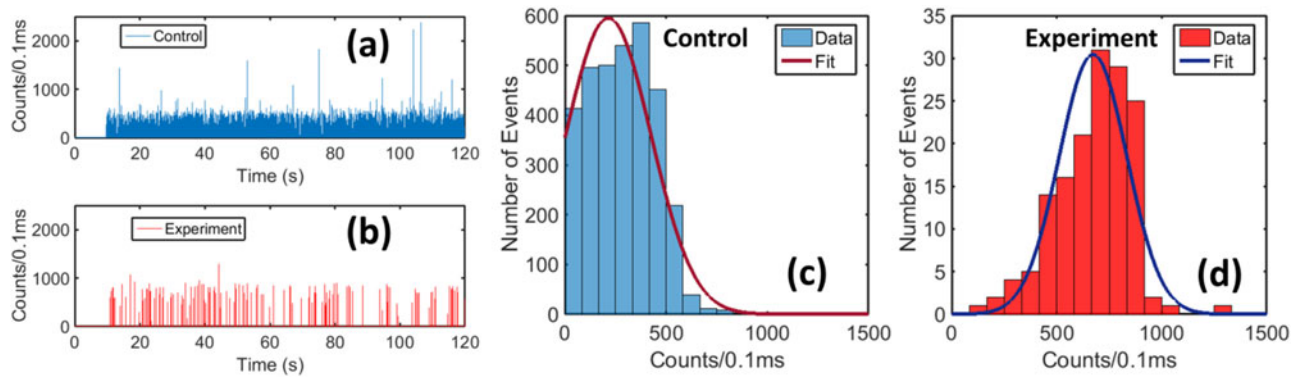


Fig. 2. (a) Fluorescence signals collected via APD for the control (no focusing) and (b) for the experiment (with focusing). (c) and (d) show the resulting peak height histograms with normal distribution fits for the control and experiment fluorescence signal heights. The fitted mean and standard deviations were found to be 214.4 and 210.6 counts per 0.1 ms for the control and 673.0 and 161.7 counts per 0.1 ms for the experiment. The CV decreases from 0.98 to 0.24 with the addition of focusing.

III. RESULTS AND DISCUSSION

A. Enhanced Detection

To quantify the enhancement due to HDF, fluorescent polystyrene beads (FluoSpheres, 500 nm diameter, yellow-green) were detected with and without focusing. An argon ion laser (488 nm) was used to excite the beads and the output light was collected as described above. Simultaneously, a microscope was used to collect video at the excitation volume from top down. Focusing experiments were performed with bead solution (concentration 3×10^7 beads/mL) in reservoir 2 and DI water in reservoirs 1 and 3. As a control experiment, bead solution was pulled through all three input reservoirs. Within the final microfluidic channel, there will exist laminar flow with a parabolic speed distribution for our experimental parameters (Poiseuille flow). Of interest are the statistics of the detected signals both with and without HDF. As discussed above, the particle's position within the microfluidic channel will alter its collection efficiency. Without HDF, particles will reside within the entire final microfluidic cross-sectional area. HDF provides a method to insert the beads into a smaller cross-sectional area where the collection efficiency is higher. Therefore, to quantify the collection efficiency statistics with and without HDF, the optical signal peak heights from the collected APD traces are analyzed with and without HDF. Fig. 2(a) and 2(b) show the raw APD traces demonstrating efficient collection of fluorescence in the chip-plane. The peaks in these APD traces correspond to signals from individual beads and their signal amplitudes (peak heights) are extracted. The resulting histograms of the fluorescence signal peak heights for the control and experiment (without and with HDF) are plotted with a fitted normal distribution in Fig. 2(c) and 2(d) respectively. We find a clear shift towards higher brightness for the experiment (Fig. 2(d)), indicating the efficacy of the focusing process. The fitted mean and standard deviations for the experimental data were found to be 673.0 and 161.7 counts per 0.1 ms. For the control, the fitted parameters are 214.4 and 210.6 counts per 0.1 ms, respectively. The resulting CVs were found to be 0.98 and 0.24 for the control and experiment respectively. The experiment showed an

improvement in CV by a factor 4.1 and an increase in the fitted mean by a factor of 3.1, demonstrating significantly enhanced detection with the addition of HDF to the optofluidic device.

As mentioned above, a video was recorded at the excitation volume while the APD trace was taken. The bead positions were fitted to extract the beads' z- and x-positions within the channel as they flowed through the excitation volume. Fig. 3(a) shows a top-down image of the z-x plane at the excitation region. The excitation solid-core waveguide lies parallel to the x-direction and guides light to the microfluidic channel in the positive x-direction. Particles flow in the positive z-direction towards the outlet reservoir. The videos demonstrate efficient focusing of the particles and can be found in the downloadable supplemental material found on <http://ieeexplore.ieee.org>. The fitted particle positions are plotted in Fig. 3(b). Both the control and experiment bead positions (blue and red in Fig. 3) were found within a small z-distribution due to the finite width of the excitation laser's mode which demonstrates effective optical guiding in the excitation waveguide.

The resulting histograms for the lateral position of the beads in the channel are found in Fig. 3(c). With the control, beads were found across the entire channel as expected. For the experiment, the beads were found to reside just off center within the microfluidic channel. Increased flow speeds would provide more sheath flow in the chip-plane, thereby forcing the particles to the perfect center of the channel. As mentioned above, only x-plane focusing was present in these experiments due to the limitation on flow speeds that would be necessary for y-direction focusing. Regardless, an enhancement in the collected optical signal is demonstrated. An increase in flow speed would result in both in- and out-of-plane focusing, thereby shrinking the velocity distribution even further and placing more of the particles within the channel at a region of high collection efficiency.

Finite element analysis was performed to calculate the theoretical particle position histograms with and without focusing for the experimentally available flow speeds (for more information on the simulation results, please see the downloadable supplemental material found on <http://ieeexplore.ieee.org>). 100

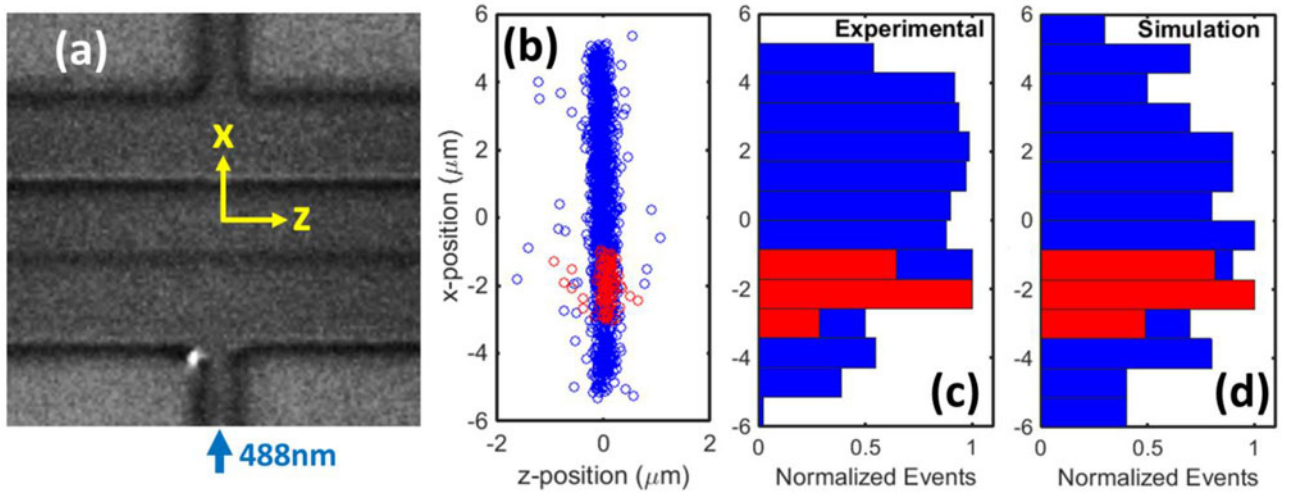


Fig. 3. (a) Top-down microscope image taken at the intersection of the solid-core excitation waveguide and the microfluidic channel. The particles flow in the $+z$ -direction and the excitation laser light propagates in the $+x$ -direction. The fluorescence signals are collected via a multi-mode solid-core waveguide downstream in the $+z$ -direction. (b) Fitted particle positions (blue and red denote control and experiment respectively) in the z - x plane found from the video as they pass through the excitation volume. The finite z -distribution is due to the waveguide confinement within the excitation waveguide. (c) The fitted experimental x -position normalized histograms for the control (blue) and experiment (red). (d) The simulated x -position normalized control (blue) and experiment (red) histograms which match very well with the experimental results.

particles were tracked for a simulated control (blue) and experiment (red) with the resulting normalized histograms found in Fig. 3(d). The HDF design is shown to force the beads towards the center of the channel as predicted by simulation. The simulated mean and standard deviation of the focused particle positions were found to be $-1.9 \mu\text{m}$ and $0.7 \mu\text{m}$, matching extremely well with the experimental results. Particle trajectories and speeds found in COMSOL were then imported into Matlab where a simulation was performed in order to predict the position dependent light collection efficiency off chip. The excitation mode profile was simulated in FIMMWAVE to predict the normalized excitation energies produced as a function of y -position and speed. The efficiency at which these excited energies are collected depends on the collection mode profile (also simulated in FIMMWAVE) and its overlap with the particle's position. These simulations suggest that perfectly centering the particle's positions within the channel ($x = 0 \mu\text{m}$) would result in $\sim 30\%$ increase in mean collected energy. Experimentally, the APD traces demonstrate enhanced detection with the implementation of 1D focusing by an increase in mean signal height and a decreased CV. Therefore, focusing is found to increase the collection efficiency of fluorescence signals from the chip. It is anticipated that further focusing in the y -direction would result in an even larger enhancement in collected optical signal.

B. Single H1N1 Virus Detection

Polystyrene bead detection as described above validates that HDF can provide enhanced detection of fluorescent particles. Of even greater interest is the detection of nanoscale biomolecules on-chip. To demonstrate enhanced detection of single viruses, H1N1 viruses were non-specifically tagged with Alexa Fluor 488 dye. As with the bead experiment, a control was run by

pulling a virus solution through all three input reservoirs and the HDF experiment was performed by pulling virus solution through reservoir 2 and nuclease-free water through reservoirs 1 and 3. Fig. 4(a) (control) and 4(b) (experiment) demonstrate for the first time optical detection of single viruses on a PDMS optofluidic platform. The resulting brightness histograms found from the APD peak heights (Fig. 4(a) and 4(b)) are plotted in Fig. 4(c) and 4(d). Note that the single viruses contain fewer fluorophores than the fluorescent polystyrene beads and therefore the resulting APD peak height histograms do not show a complete normal distribution. Therefore, the plotted fits are an exponential decay with decay rates of 0.020 and 0.014 in units of 0.1 ms bin time per counts for the control and experiment. However, the mean signal height was found to be 94.8 counts per 0.1 ms for the control and 155.9 counts per 0.1 ms for the experiment. Thereby, an enhanced mean signal height of a factor 1.64 is demonstrated with the addition of HDF on chip.

Though the full distribution is not present in the detected APD peak heights, the speed distributions were determined via fluorescence correlation spectroscopy (FCS). For each peak found in the APD trace, the FCS autocorrelation trace, $G(\tau)$, was fit to extract the virus's speed [26], [27]. Fig. 5(a) plots three such normalized autocorrelation traces with fits from the control data. The resulting speed histograms with fits for the control and experiment are plotted in Fig. 5(b) and 5(c). The resulting mean speeds for the control and experiment were found to be 4.5 and 3.7 cm/s, respectively. The slower mean speed for the experiment is to be expected due to the slight offset of the focusing from the center of the microfluidic channel. The standard deviations were found to be 0.73 and 0.54 cm/s for the control and experiment. The speed distribution is substantially narrower for the in-plane focusing and could be decreased further with the addition of focusing out of the chip-plane (y -direction).

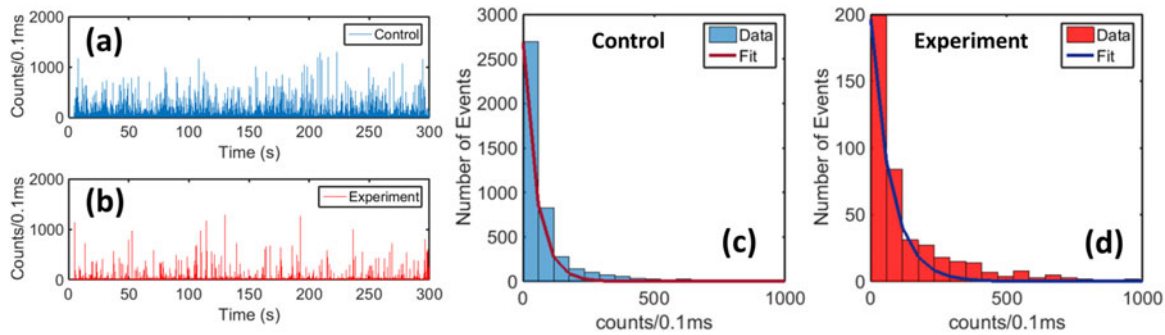


Fig. 4. (a) H1N1 fluorescence signals collected via APD for the control and (b) for the experiment. (c) and (d) show the resulting histograms with exponential decay fits for the control and experiment fluorescence signal heights. The mean signal height for the control and experiment are 94.8 and 155.9 counts per 0.1 ms, respectively demonstrating enhanced detection of a factor 1.64.

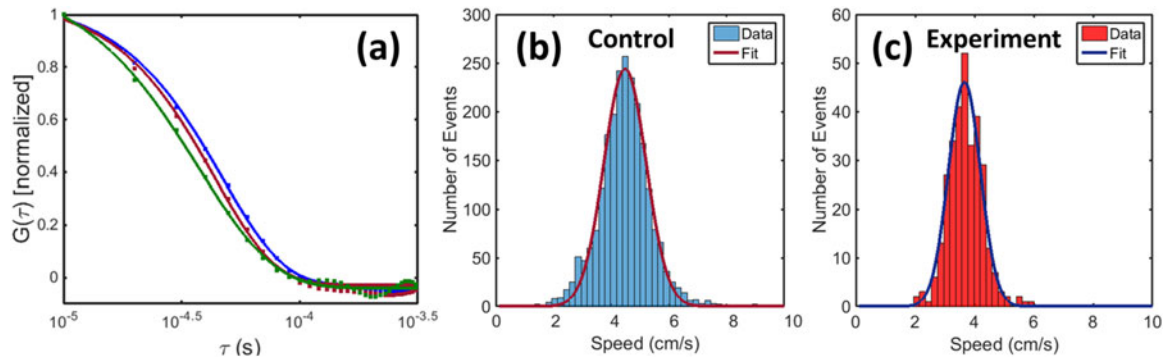


Fig. 5. (a) Sample normalized FCS autocorrelation curves, $G(\tau)$, with fits for three signals within the control data trace. (b) and (c) show the fitted speed histograms for the control and experiment traces respectively. The fitted means are 4.5 and 3.7 cm/s for the control and experiment. The fitted standard deviations are 0.73 and 0.54 cm/s for the control and experiment demonstrating a narrower velocity distribution due to focusing in the chip-plane.

IV. CONCLUSION

The addition of lateral HDF to a planar PDMS based optofluidic device was found to enhance the detection of fluorescence signals on-chip. Fluorescent polystyrene bead experiments demonstrated a decrease in CV with the addition of HDF and an increase in the mean signal height collected from the chip. Further, the devices were found to have sufficient sensitivity to detect single viruses on-chip. The addition of HDF to the PDMS based devices resulted in an increase in the mean signal height of H1N1 experiments by a factor of 1.64. A larger enhancement is anticipated for stronger focusing towards the center of the collection channel. Further, out of plane focusing could be implemented by pushing the particles through the chip at higher speeds. This design is compatible with silicon-based platforms and could readily be transferred to optofluidic platforms based on silicon or other materials. Further, on-chip whole blood cell filtration and fluorescent labelling has been demonstrated and such an architecture can be implemented with the presented HDF design for a near front-to-back point of care optofluidic device [2].

ACKNOWLEDGMENT

The authors would like to acknowledge A. Stambaugh for the labeling of H1N1 viruses. The authors would also like to thank G. Meena and A. Jain for useful discussions.

REFERENCES

- [1] H. Schmidt and A. R. Hawkins, "The photonic integration of non-solid media using optofluidics," *Nat. Photon.*, vol. 5, no. 10, pp. 598–604, Oct. 2011.
- [2] H. Cai *et al.*, "Optofluidic analysis system for amplification-free, direct detection of Ebola infection," *Sci. Rep.*, vol. 5, Sep. 2015, Art. no. 14494.
- [3] D. Ozcelik, H. Cai, K. D. Leake, A. R. Hawkins, and H. Schmidt, "Optofluidic bioanalysis: Fundamentals and applications," *Nanophotonics*, vol. 6, no. 4, pp. 647–661, Jul. 2017.
- [4] D. Ozcelik *et al.*, "Scalable spatial-spectral multiplexing of single-virus detection using multimode interference waveguides," *Sci. Rep.*, vol. 7, no. 1, Sep. 2017, Art. no. 12199.
- [5] S. Liu *et al.*, "Electro-optical detection of single λ -DNA," *Chem. Commun.*, vol. 51, no. 11, pp. 2084–2087, Jan. 2015.
- [6] T. Fujii, "PDMS-based microfluidic devices for biomedical applications," *Microelectron. Eng.*, vol. 61, pp. 907–914, Jul. 2002.
- [7] S. Metz, S. Jiguet, A. Bertsch, and P. Renaud, "Polyimide and SU-8 microfluidic devices manufactured by heat-depolymerizable sacrificial material technique," *Lab. Chip*, vol. 4, no. 2, pp. 114–120, Jan. 2004.
- [8] K. Liu and Z. Hugh Fan, "Thermoplastic microfluidic devices and their applications in protein and DNA analysis," *Analyst*, vol. 136, no. 7, pp. 1288–1297, Jan. 2011.
- [9] E. Fu and C. Downs, "Progress in the development and integration of fluid flow control tools in paper microfluidics," *Lab. Chip*, vol. 17, no. 4, pp. 614–628, Jan. 2017.
- [10] C. W. Tsao, L. Hromada, J. Liu, P. Kumar, and D. L. DeVoe, "Low temperature bonding of PMMA and COC microfluidic substrates using UV/ozone surface treatment," *Lab. Chip*, vol. 7, no. 4, pp. 499–505, Mar. 2007.
- [11] G. M. Whitesides, "The origins and the future of microfluidics," *Nature*, vol. 442, no. 7101, pp. 368–373, Jul. 2006.
- [12] S. K. Sia and G. M. Whitesides, "Microfluidic devices fabricated in poly(dimethylsiloxane) for biological studies," *Electrophoresis*, vol. 24, no. 21, pp. 3563–3576, Nov. 2003.

- [13] Y. K. Suh and S. Kang, "A Review on mixing in Microfluidics," *Micro-machines*, vol. 1, no. 3, pp. 82–111, Sep. 2010.
- [14] H.-D. Xi *et al.*, "Active droplet sorting in microfluidics: A review," *Lab. Chip*, vol. 17, no. 5, pp. 751–771, Feb. 2017.
- [15] S.-Y. Teh, R. Lin, L.-H. Hung, and A. P. Lee, "Droplet microfluidics," *Lab. Chip*, vol. 8, no. 2, pp. 198–220, Jan. 2008.
- [16] G.-B. Lee, C.-C. Chang, S.-B. Huang, and R.-J. Yang, "The hydrodynamic focusing effect inside rectangular microchannels," *J. Micromech. Microeng.*, vol. 16, no. 5, pp. 1024–1032, Apr. 2006.
- [17] X. Mao, S.-C. Steven Lin, C. Dong, and T. Jun Huang, "Single-layer planar on-chip flow cytometer using microfluidic drifting based three-dimensional (3D) hydrodynamic focusing," *Lab. Chip*, vol. 9, no. 11, pp. 1583–1589, Mar. 2009.
- [18] X. Mao *et al.*, "An integrated, multiparametric flow cytometry chip using 'microfluidic drifting' based three-dimensional hydrodynamic focusing," *Biomicrofluidics*, vol. 6, no. 2, Apr. 2012, Art. no. 024113.
- [19] D. Ozelik *et al.*, "Signal-to-noise enhancement in optical detection of single viruses with multispot excitation," *IEEE J. Sel. Top. Quantum Electron.*, vol. 22, no. 4, pp. 6–11, Jul. 2016.
- [20] D. Ozelik *et al.*, "Optofluidic wavelength division multiplexing for single-virus detection," *Proc. Nat. Acad. Sci. USA*, vol. 112, no. 42, pp. 12933–12937, Oct. 2015.
- [21] H. Chandralahim and X. Fan, "Reconfigurable solid-state dye-doped polymer ring resonator lasers," *Sci. Rep.*, vol. 5, Dec. 2015, Art. no. 18310.
- [22] J. W. Parks and H. Schmidt, "Flexible optofluidic waveguide platform with multi-dimensional reconfigurability," *Sci. Rep.*, vol. 6, Sep. 2016, Art. no. 33008.
- [23] P. G. Hermansson *et al.*, "All-polymer photonic crystal slab sensor," *Opt. Express*, vol. 23, no. 13, pp. 16529–16539, Jun. 2015.
- [24] D. D. Carlo, "Inertial microfluidics," *Lab. Chip*, vol. 9, no. 21, pp. 3038–3046, Sep. 2009.
- [25] Z. Cai, W. Qiu, G. Shao, and W. Wang, "A new fabrication method for all-PDMS waveguides," *Sens. Actuators A, Phys.*, vol. 204, pp. 44–47, Dec. 2013.
- [26] D. Yin, E. J. Lunt, M. I. Rudenko, D. W. Deamer, A. R. Hawkins, and H. Schmidt, "Planar optofluidic chip for single particle detection, manipulation, and analysis," *Lab. Chip*, vol. 7, no. 9, pp. 1171–1175, Aug. 2007.
- [27] D. Yin, E. J. Lunt, A. Barman, A. R. Hawkins, and H. Schmidt, "Microphonic control of single molecule fluorescence correlation spectroscopy using planar optofluidics," *Opt. Express*, vol. 15, no. 12, pp. 7290–7295, Jun. 2007.



Jennifer A. Black (S'12) received the B.S. degree in physics from Southern Polytechnic State University, Marietta, GA, USA, in 2010, and the M.S. degree in physics from the University of California Santa Cruz, Santa Cruz, CA, USA, in 2014. She is currently working toward the Ph.D. degree in electrical engineering at the University of California Santa Cruz. Her research interests include waveguide based light-matter interactions, slow and stored light in warm atomic vapor, and chip-based interferometry. She has been a Member of the Applied Optics Group, University of California Santa Cruz since 2011. She is a student member of the Optical Society. She is also a National Science Foundation Graduate Research Fellow.



Erik Hamilton received the B.S. degree in electrical and computer engineering from Brigham Young University, Provo, UT, USA, in 2015. He is currently working toward the Ph.D. degree in electrical and computer engineering at Brigham Young University. From 2014 to 2015, he was a Research Assistant with the Ira A. Fulton College of Engineering, Tempe, AZ, USA. His research interest focuses on biooptofluidics, with expertise in the design, fabrication, and characterization of integrated optofluidics, specifically single molecule detection by three-dimensional hydrodynamic focusing.



Raúl A. Reyes Hueros is working toward the B.S. degree in both applied physics and computational mathematics at the University of California Santa Cruz (UCSC), Santa Cruz, CA, USA. He was a Member of the Applied Optics Group at UCSC since January 2017. His current research interests include molecular biology, design, simulations, and integration of optofluidic devices and Bragg gratings. He is the recipient of a National Science Foundation stipend.



Joshua W. Parks received his B.S. degree in biochemistry from the University of Portland, OR, USA, in 2010, and the M.S. degree in biochemistry from the University of California Santa Cruz (UCSC), Santa Cruz, CA, USA, in 2012, and the Ph.D. degree in electrical engineering from UCSC in 2016. His research interests include design, fabrication, and characterization of integrated biophotonic, reconfigurable optofluidic, and clinical biosensing devices. He is the recipient of the Eugene Cota Robles Fellowship, the National Science Foundation Graduate Research Fellowship Program (NSF-GRFP) fellowship, and the Research Mentoring Institute fellowship.



Aaron R. Hawkins (F'16) received the B.S. degree in applied physics from the California Institute of Technology, CA, USA, in 1994, and the M.S. and Ph.D. degrees in electrical and computer engineering from the University of California, Santa Barbara, CA, USA, in 1996 and 1998, respectively. He was a Cofounder of Terabit Technology and was later at CIENA and Intel. He is currently a Professor with the Electrical and Computer Engineering Department, Brigham Young University, Provo, UT, USA. He has authored or co-authored more than 300 technical publications. He is a Fellow of the OSA and is currently the Vice-President of publications for the IEEE Photonics Society.



Holger Schmidt (F'17) received the Ph.D. degree in electrical and computer engineering from the University of California Santa Barbara, Santa Barbara, CA, USA. He was a Postdoctoral Fellow with the Massachusetts Institute of Technology, Cambridge, MA, USA. He is the Narinder Kapany Chair of Optoelectronics, Professor of Electrical Engineering, and Associate Dean for Research with the Baskin School of Engineering, University of California Santa Cruz, Santa Cruz, CA, USA. His research interests include photonics and integrated optics, including optofluidic devices, atom photonics, nano-magneto-optics, nonlinear optics, and ultrafast optics. He has authored or co-authored 400 publications, coedited the *CRC Handbook of Optofluidics*, and serves on the Editorial Board for Scientific Reports. He is a Fellow of the OSA, and the recipient of an NSF Career Award and a Keck Futures Nanotechnology Award.